AGU PUBLICATIONS

Geophysical Research Letters

RESEARCH LETTER
10.1002/2016GL069267

Key Points:
- New LF method to image the 3-D structure and dynamics of intracloud initial upward negative leader
- First LF technique to distinguish initial pulses from main channel and from nonpropagating branches
- Tilted initial leader channel with average 3-D step length of ~295 m and step interval of 1.05 ms

Correspondence to:
S. A. Cummer,
cummer@ee.duke.edu

Citation:
Lyu, F., S. A. Cummer, G. Lu, X. Zhou, and J. Weinert (2016), Imaging lightning intracloud initial stepped leaders by low-frequency interferometric lightning mapping array, *Geophys. Res. Lett.*, *43*, doi:10.1002/2016GL069267.

Received 12 FEB 2016
Accepted 13 MAY 2016
Accepted article online 16 MAY 2016

Imaging lightning intracloud initial stepped leaders by low-frequency interferometric lightning mapping array

Fanchao Lyu[1], Steven A. Cummer[1], Gaopeng Lu[2,3], Xuan Zhou[4], and Joel Weinert[1]

[1]Electrical and Computer Engineering Department, Duke University, Durham, North Carolina, USA, [2]Key Laboratory of Middle Atmosphere and Global Environment Observation, Institute of Atmospheric Physics, Chinese Academy of Sciences, Beijing, China, [3]Collaborative Innovation Center on Forecast and Evaluation of Meteorological Disasters, Nanjing University of Information Science and Technology, Nanjing, China, [4]Department of Electrical Engineering, Tsinghua University, Beijing, China

Abstract By comparing the source position of pulses during initial leaders and the paths of subsequent dart leaders from typical bilevel intracloud (IC) flashes, we demonstrate a new method to image the detailed three-dimensional (3-D) structure and stepping dynamics of IC initial leaders. Using this approach, we show that nearly half of the initial breakdown pulses are not involved in the main channel extension but instead originate in nonpropagating branches. The primary upward but significantly tilted initial leader channels propagated with measured mean/median 3-D step length of 295/265 m and mean/median step interval of 1.05/0.6 ms. The structure and dynamics of IC initial upward negative leaders are distinct from those of highly branched cloud-to-ground downward negative leaders. We suggest that the tilted initial leader channel and electric field could affect the observation on leader-associated high-energy radiation phenomena, such as the position-dependent observation of terrestrial gamma ray flashes from space-based detectors.

1. Introduction

In the past several decades, the main features of intracloud (IC) flashes and the incloud processes during cloud-to-ground (CG) flashes were resolved by the development of radio-based lightning mapping arrays operating at either high frequency/very high frequency (HF/VHF) [e.g., *Proctor*, 1981; *Proctor et al.*, 1988; *Mazur*, 1989; *Rhodes et al.*, 1994; *Shao and Krehbiel*, 1996; *Rison et al.*, 1999; *Kawasaki et al.*, 2000; *Dong et al.*, 2002; *Qiu et al.*, 2009; *Zhang et al.*, 2010; *Liu et al.*, 2012; *Stock et al.*, 2014; *Sun et al.*, 2014] or low frequency (LF) [e.g., *Betz et al.*, 2004; *Marshall et al.*, 2013; *Bitzer et al.*, 2013; *Karunarathne et al.*, 2013; *Lyu et al.*, 2014; *Yoshida et al.*, 2014; *Wu et al.*, 2015; *Wang et al.*, 2016]. A normal positive IC flash often starts with an initial negative leader that creates an upward channel bridging the negative and positive charge layers then horizontally extends into the two layers. However, the stepping feature of IC initial leaders is not yet fully understood. The significance of IC initial leader stepping measurements is evident, which yields better insight into lightning initiation and the structure and dynamics of IC initial leaders, as well as the physical mechanism of IC leader associated phenomena like gigantic jets and terrestrial gamma ray flashes.

A few rare photographic reports of cloud-to-air discharges [*Krehbiel et al.*, 2008; *Edens et al.*, 2014] and leaders in virgin air under the cloud base [*Montanyà et al.*, 2015] have shown propagation features of IC leaders outside the cloud. From color photographs captured of parts of IC flashes out of the cloud, *Edens et al.* [2014] found that the relatively straight segments of the IC leader steps had a length of at least 200 m at the altitude of ~10 km when the leader developed into the clear air. These images also clearly showed the stepping segments and some nonpropagating branches along the main channel. Because of the opacity of the cloud, however, much of the channel was hidden within the cloud. While photographic observations are highly effective for studying CG stepped leaders, similar observations are normally unavailable for IC stepped leaders (except for those special cases noted above).

Previous studies have demonstrated that radio-based lightning mapping arrays are extremely capable for mapping entire flashes and some smaller scale processes, but few have focused in detail on the IC initial leader stepping structure and dynamics. IC leader step lengths were estimated in the range of 50–600 m from coordinated observation by balloon-borne electric field instrument and the lightning mapping array (LMA)

[*Winn et al.*, 2011]. Using a low-frequency (LF) mapping array, *Wu et al.* [2015] analyzed the detailed characteristics of initial breakdown pulses. By assuming no branches and only vertical propagation of initial leader, they estimated the average step length during IC initial leaders to be 113 m from the pulse rate and average upward propagation speed. Note that negative leaders from cloud-to-air flashes [*Edens et al.*, 2014], and downward stepped leaders from CGs [e.g., *Hill et al.*, 2011; *Lu et al.*, 2012; *Stolzenburg et al.*, 2014] are usually accompanied by luminous branches, each of which may be associated with LF pulse [*Stolzenburg et al.*, 2014]. Therefore, in order to better understand initial IC leaders and the stepping features of these upward channels, more results from lightning imaging systems operating at either HF/VHF or LF frequency regime are still needed and valuable.

Here we present a new approach that combines the source locations from initial breakdown pulses during the initial leader and from subsequent dart leaders to image the upward stepping dynamics and structure during initial IC leaders. We demonstrate this concept using measurements from our LF near-field interferometric-TOA (time-of-arrival) lightning mapping array (LFI-LMA) [*Lyu et al.*, 2014]. Three scientific results from initial upward leader imaging are presented to demonstrate the capability of this approach. Our results suggest that nearly half of the initial breakdown pulses (often smaller amplitude pulses) seem to be from the nonpropagating branches during the upward channel development. The main channel extended with an average step length of 295 m and often with a significant tilt from vertical of several tens of degrees. To the best of our knowledge, this is the first investigation of the structure and dynamics of the IC initial upward channel by the combination of LF pulse source positions from initial leader and subsequent dart leader from lightning imaging systems.

2. Combining Source Locations From Initial Breakdown Pulses and Subsequent Dart Leaders

Our approach exploits the fact that some IC dart leaders follow the existing path propagating back toward the flash origin and through the upward channel built by the initial leader to the upper positive charge layer [*Shao and Krehbiel*, 1996]. Benefiting from the continuous data recording and the interferometric data processing methods, the LFI-LMA is capable of mapping both the discrete pulses during initial leaders and the continuous emissions during dart leader processes [*Lyu et al.*, 2014]. From the combination of the LF source positions from the initial breakdown pulses (IBPs, pulses during the first few tens of milliseconds [*Shao and Krehbiel*, 1996; *Marshall et al.*, 2013]) and the subsequent continuous path from dart leaders, it is possible for us to distinguish the IBPs along the upward channel and those away from the channel, which in turn enables us to accurately image the stepping and structure of the upward channel.

In addition to the automated processing method that is used to map the whole flash and to find the special features during a flash, we applied two other processing steps to improve the LF source time finding for IBPs and subsequent dart leaders, respectively.

1. Pulse-peak finding. We measured the individual pulse peak times within each IBP. All the IBPs with peak amplitude greater than the noise level are processed. This time finding method on discrete pulses is similar to the application by previous reports [e.g., *Bitzer et al.*, 2013; *Karunarathne et al.*, 2013; *Yoshida et al.*, 2014] and, in this case, increases the number of discrete source locations found.
2. Two-step interferometric parsing. An improved automated average source time difference finding method was applied to LFI-LMA during the dart leaders when continuous emission dominated. This contains two specific parsing steps when finding the time difference from each two LF sensors. In the first step, which is the same as the method described by *Lyu et al.* [2014], a 350 μs sliding window cross correlation is used to find the average time difference for that window. In the second step, the signals in the 350 μs window were shifted with the time difference found in the first step, and then a smaller sliding window (50 μs) cross correlation was further applied to the time-shifted LF signals. In this way, more individual source points of the dart leader are found. This method is especially useful when applied to continuous emissions.

These two-source time finding methods and the fully automated method applied by *Lyu et al.* [2014] were compared on LF signals in a 700 μs window from two LF sensors. The difference between the average time of manually pulse-peak finding and method applied by *Lyu et al.* [2014] is 0.31 μs, while the difference between the average time of manually pulse-peak finding and the two-step interferometric parsing is

0.16 μs. Both are comparable to the system time accuracy (~0.4 μs) [*Lyu et al.*, 2014], which indicated that the location results by time of arrival from these three methods are consistent with each other.

The pulse-peak finding method was applied to the IBPs to find the peak time of every discrete pulse above noise level, and then the peak time differences of the discrete pulses from each two LF sensors were computed. The two-step interferometric parsing was applied to the dart leaders to find the windowed average time differences of continuous emissions from each pair of LF sensors. Then the TOA method was applied to these time differences to find the 3-D positions of both IBPs (x, y, h) and dart leaders (X, Y, H). As mentioned above, we assume that the main upward channel created by initial leaders and the channel followed by subsequent dart leader are the same. Thus, identifying the main channel steps and distinguishing them from nonpropagating branches is relatively straightforward. A source position comparison between each discrete IBP source (x_i, y_i, h_i, $i = 1, \ldots, N$) and the path of dart leader sources (X, Y, H) was conducted by the following criteria to find the IBPs sources which best-fitted the dart leader path:

$$\mathrm{MIN}\left(\sqrt{(x_i - X|_{H\le h_i})^2 + (y_i - Y|_{H\le h_i})^2 + (h_i - H|_{H\le h_i})^2}\right) \le 200\ m\ (i = 1, \ldots, N)$$

where N is the total number of locatable IBPs. Because the conductive dart leader channels can only exist where the IBPs built the path, we thus take the 3-D distance between each IBP (x_i, y_i, h_i) and the closest located point along the dart leader path up to the altitude of the IBP. If the closest 3-D distance is less than 200 m, then this IBP (x_i, y_i, h_i) was considered to be a "node" along the channel, while if the minimum distance is greater than 200 m, then it was grouped into the side branches. We then repeat this for all IBPs.

This 200 m is determined by the 3-D location error within the LFI-LMA network [*Lyu et al.*, 2014] and is consistent with the distance distribution of all the IBP positions to the dart leader channel (which is a bimodal-like distribution, with the two groups separated by around 200 m). The minimum distances of all the nodes to the dart leaders in this study have a mean value of 83 m, which is much smaller than the estimated location error.

We recognize that the source of a particular LF pulse could involve a larger region than the source location of a VHF pulse. The exact nature of the LF pulse source region is still unclear, and this assumption that the LF pulse was from the point position may not be valid. However, a point position from the pulse peak time can be calculated and thus can describe the typical source of an LF pulse, as also applied by previous studies [*Bitzer et al.*, 2013; *Karunarathne et al.*, 2013; *Yoshida et al.*, 2014; *Wu et al.*, 2015]. In fact, from the comparison between the point position of IBPs and the dart leader channel, the conductive channel appears to change directions at the IBP point locations, which we refer to as nodes. Thus, it is reasonable for us to assume that the peak of the LF pulse was from a node when an individual step was completed rather than to suppose it was from somewhere during the middle of step. Next, each step is defined to be the process between two neighboring nodes. Note that since the step lengths were measured by comparing the path of dart leaders, the actual initiation IBP of the initial leader may not be involved in the step lengths measurement.

We applied this approach to six IC flashes that occurred within the LFI-LMA network with good location accuracy (both horizontal and height location accuracy less than 200 m, with best location accuracy of 50–100 m [*Lyu et al.*, 2014]) and had well-defined lightning initial and dart leaders (including the two examples shown in the following section) to demonstrate its capability.

3. Two Examples of Initial IC Leader Imaging

Figure 1 illustrates an image of a typical normal polarity bilevel IC flash that occurred on 11 June 2014 at 22:23:20 (UTC) (Flash 1). A total of 1238 LF sources were mapped during this 900 ms IC flash, as illustrated in Figures 1a–1c. Flash 1 started with an upward negative leader initiated at 8.3 km above ground level (agl) and continued ascending to 11.9 km agl in the first 30 ms. The LF source distribution conveys the existence of two charge layers during the flash, one negative layer at 5–7 km and another positive layer at 7–12 km in different horizontal regions. The negative leader channels in the upper positive charge layer are much better organized than the paths relating to the positive leaders in the lower negative charge layer. Figures 1d–1f illustrate the LF waveforms and the source positions of IBPs and dart leaders. The IBPs involved in the main channel stepping, again identified by ≤200 m distance from the dart leader channel, are shown by color circled dots in Figure 1d, and also color circled and connected by the magenta line in Figure 1f. Some LF

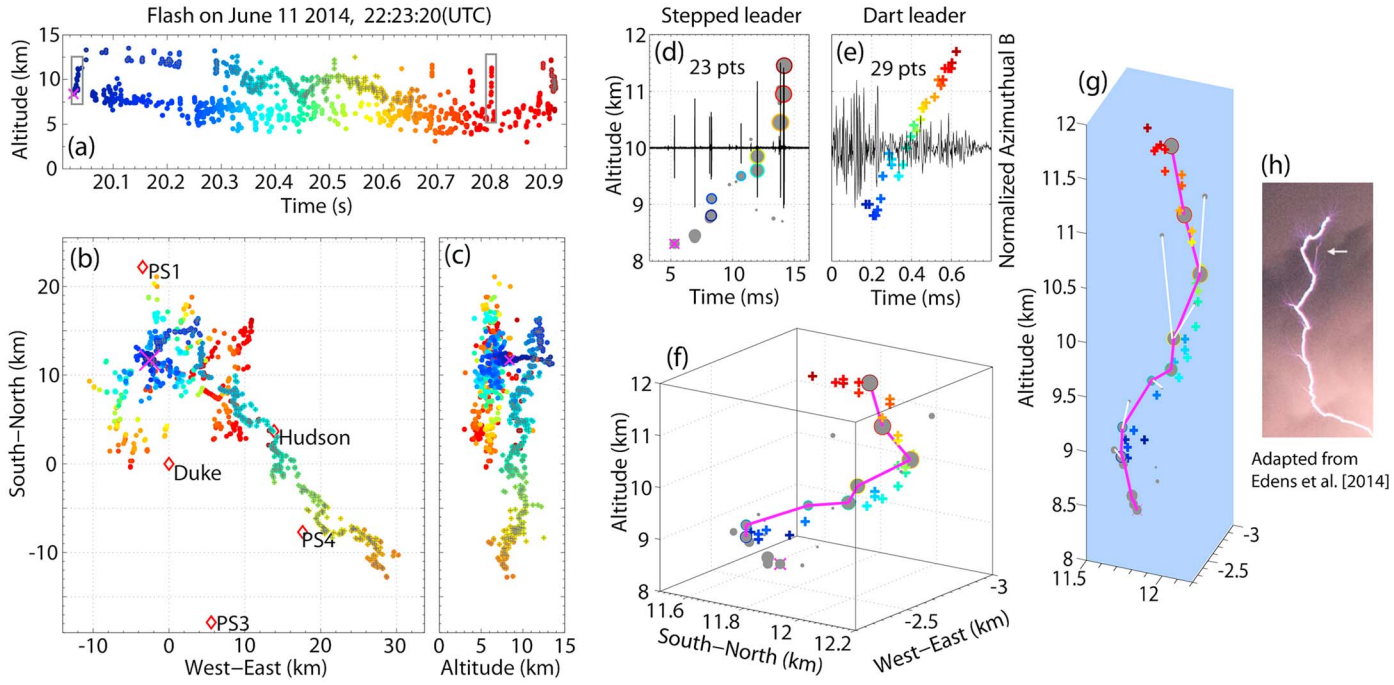

Figure 1. The development of a normal IC flash and the initial leader structure mapped by the combination of IBPs and subsequent dart leaders. (a) LF source altitude during the flash development, the color from blue to red indicating the time variation from flash beginning to end. (b) Plan view of the whole flash. (c) Vertical view of flash from west to east. (d) LF waveform and altitudes of locatable IBPs. The size of the gray dots indicates the relative amplitude of the pulses, and color circled dots illustrate those involved in channel stepping. (e) LF waveform and altitudes of dart leader ("+") process of dart leader. The two black rectangles in Figure 1a mark the initial leader and dart leader processes in Figures 1d and 1e. (f) A 3-D view of the paths mapped from IBPs (shown in Figure 1d) and dart leader (shown in Figure 1e), with a magenta line connecting the IBPs along the dart leader path. (g) A 3-D image of the possible main channel (magenta line) starting from the first locatable IBP and the possible nonpropagating branches (grey dots connected by the white segments). (h) A photo captured by *Edens et al.* [2014] illustrates the leader channel propagating outside the cloud. Note that the temporal color scale in Figures 1a–1c is the same but changes in Figures 1d and 1e.

sources, especially those from small IBPs, are not involved in the main channel stepping. We suggest that these sources are associated with the nonpropagating branches during the development of the upward channel, similar to the photographic observations of cloud-to-air flashes [*Edens et al.*, 2014]. Note that the initial IC leader stepping structure and dynamics mapped by LFI-LMA agrees well with the reported cloud-to-air leader photo from many aspects, as illustrated by visual comparison between our image and the photo captured by *Edens et al.* [2014] in Figures 1g–1h.

Figure 2 illustrates the mapping results from another bilevel IC flash (Flash 5) which occurred on 20 April 2015 at 22:23:52 (UTC). The initial leader in Flash 5 propagated upward from ~5.4 km to 8.3 km. The whole picture of initial leaders and dart leaders shows a similar dynamic structure to that of Flash 1. Again, most sources with relatively small amplitude were away from the dart leader path and thus assumed to be from nonpropagating branches. Similar to Figure 1, the whole channel extended upward in a stepped structure, tilted significantly from vertical, which was followed by the subsequent dart leaders from the bottom to top.

4. New Findings on Initial IC Leaders

As illustrated in the above two examples, by combining the source position of IBPs and the subsequent dart leaders, our approach showed several aspects of the detailed structure and dynamics of the initial leaders of which little was previously known, including step length (distance between neighboring nodes) and inter-step time interval; separate identification of the pulses associated with the main channel extension and side branches; and the degree of tilt from vertical of the initial upward channel. Table 1 summarizes the main scientific results measured from six IC flashes. For all six flashes, as a comparison to previous studies, the measured average velocity of initial leaders (ranging from 0.9 to 5.0×10^5 m/s) and average velocity of dart leaders (ranging from 0.9 to 7.1×10^6 m/s) agree well with the results from the LMA and VHF interferometry [e.g., *Shao and Krehbiel*, 1996; *Behnke et al.*, 2005; *Stock et al.*, 2014].

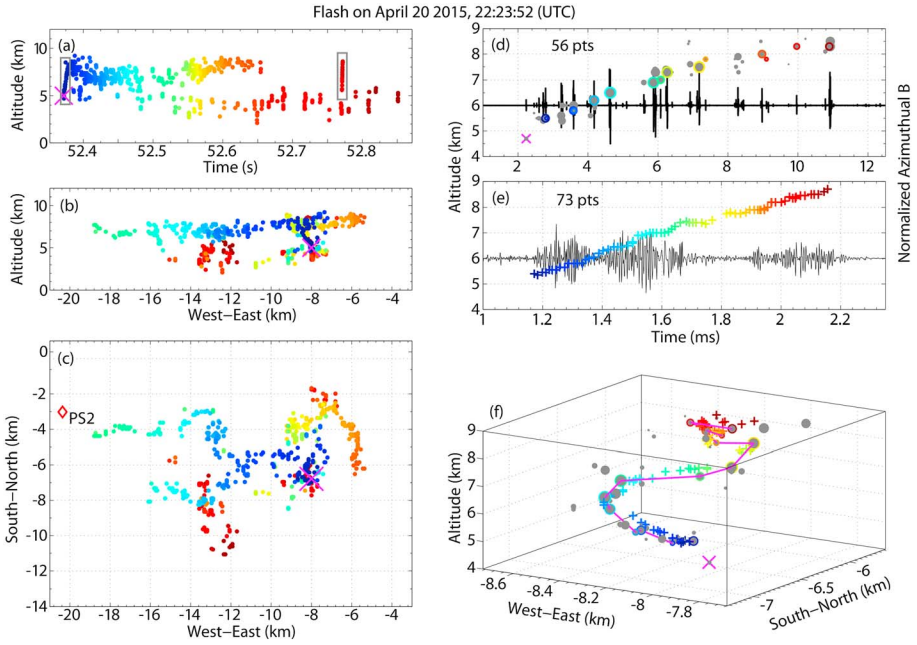

Figure 2. LF source locations and the leader stepping structure for another normal IC flash. The signs have the same meaning as those shown in Figure 1. (a) LF source location during the development of the flash, with two black rectangles marking the initial leader stage and the subsequent dart leader process, respectively. (b) Vertical view of the flash from south to north. (c) Plan view of the whole flash. (d–f) Same format as in Figure 1. Note that the color scale in Figures 2a–2c is the same but changes in Figures 2d and 2e.

Figures 3a and 3b illustrate the step length and interstep time interval distribution. In all six flashes, the measured step length along the channel ranged from 56 m to 806 m, with 82% of the step lengths in this study between 100 m and 500 m. We suggest that this could be the typical streamer zone length of initial IC negative leaders. The mean/median step length is 295/265 m, which is much longer than that from the initial breakdown stage of CG flashes [*Stolzenburg et al.*, 2014], but comparable to the ~200 m step length from recent photographic observation on cloud-to-air leaders by *Edens et al.* [2014] and the 50–600 m step length measured from LMA and a balloon-borne electric field instrument by *Winn et al.* [2011]. The mean/median step time interval in this study is 1.05/0.6 ms, while the mean/median pulse time interval during the leader process is 0.56/0.13 ms. We recognize that this is an upper bound because some weak pulses may not always be identified and located. The step length measured here is somewhat larger than reported recently by *Wu et al.* [2015], who assumed that every pulse was a forward step. If we follow this assumption, then 0.56 ms per pulse combined with the average leader 3-D propagation speed of 2.8×10^5 m/s measured here gives an average 3-D step length of 157 m, which agrees reasonably well with the 113 m average step length from

Table 1. Summary of the Measured Parameters During the Initial Leaders From Six Flashes

Flash No.	All	1	2	3	4	5	6
Source altitude (km)	5.4–11.5	8.8–11.5	8.1–9.9	9.1–10.8	7.2–10.0	5.4–8.3	9.2–10.3
Initial stepped leader average 3-D velocity ($\times 10^5$ m/s)	2.8	4.8	0.9	1.9	2.9	5.0	2.0
Dart leader average 3-D velocity ($\times 10^6$ m/s)	3.2	6.3	4.0	2.4	7.1	4.1	0.9
Min/max step length (m)	56/806	67/691	114/495	65/806	88/562	56/496	172/438
Mean/median step length (m)	295/265	406/512	252/207	276/213	287/293	290/318	320/353
Mean/median step interval (ms)	1.05/0.60	0.85/0.24	2.99/1.09	1.45/3.82	0.99/0.91	0.58/0.33	1.64/1.68
Mean/median pulse interval[a] (ms)	0.56/0.13	0.41/0.09	0.66/0.30	0.18/0.07	0.49/0.11	0.44/0.16	0.88/0.47
Averaged each step angle/overall channel angle[b] (°)	–	21/11	29/35	31/38	36/11	40/17	27/6

[a]All the locatable pulses during the initial leaders.
[b]The angle means the tilt angle relative to the vertical direction. The angle of each step means the tilt of each step segment, while overall channel angle means the tilt between the first and the last leader sources involved in channel stepping.

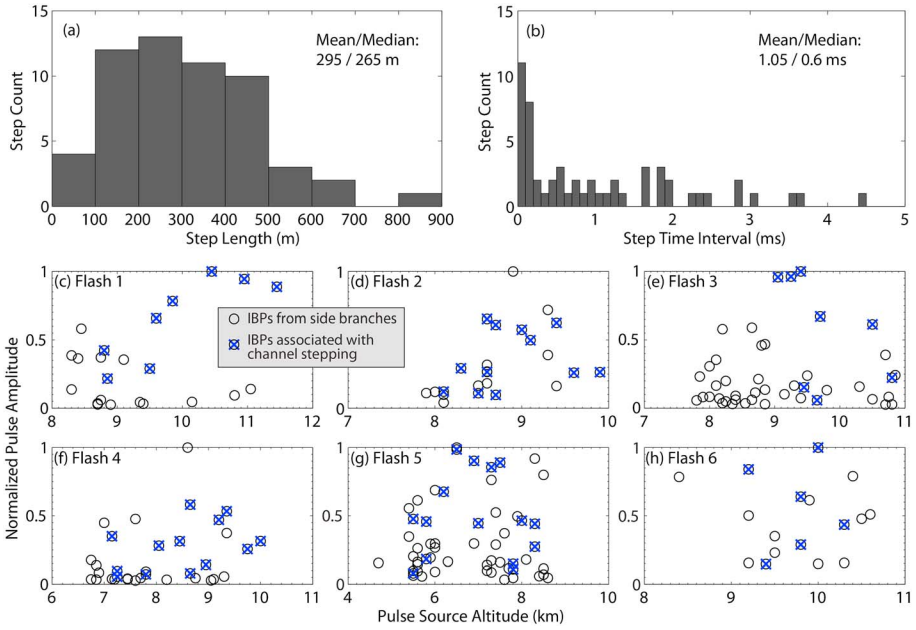

Figure 3. The distribution of step length, time interval, and pulse amplitude of IBPs during the initial leader progression. (a) Step length distribution. (b) Step time interval distribution. (c–h) Normalized amplitude of IBPs (vertical axes) with the progression of initial leader (horizontal axes). The back circles with blue crosses indicate the IBPs associated with the channel stepping, while the empty black circles show the IBPs identified as side branches.

Wu et al. [2015]. Our ability to distinguish forward steps and side branches results in better estimates of the step length and interstep time interval that are about two times larger.

Figures 3c–3h show the normalized amplitude of the IBPs during the progression of the six initial leaders as a function of altitude, separating those points on the main channel from those on nonpropagating branches. In most cases, the largest pulses usually appear during the middle or final stage of the initial leader and are usually (but not always) associated with main channel stepping. Some high-amplitude pulses were not identified as channel nodes, however. The detailed relationship between the pulse amplitude and channel stepping is not very clear, and it is difficult for us to draw a firm conclusion on the relationship between pulse amplitude and stepping formation based on the small sample reported here. However, qualitatively, we see that high-amplitude pulses are more likely to contribute to the development of the leader channel, while lower-amplitude pulses are more likely to be associated with nonpropagating branches.

We also investigated the upward progression of the individual steps and the whole channel. The very initial steps of leaders were not analyzed here because of the lack of a comparable dart leader path. However, after the first ~500 m of the upward negative leader, it took an average of another ~9 steps (ranging from 5 to 14 steps) for all the leaders to reach the channel top as shown in Figures 3c–3h. Each step progressed with an average angle of 21° to 40° from the vertical direction. The overall tilt from vertical of the complete upward channel varied from 6° to 38°, as illustrated in Table 1.

5. Implications and Summary

By applying improved LF pulse source finding methods to the LFI-LMA [*Lyu et al.*, 2014] and directly comparing the source positions mapped from the pulses of initial upward negative leaders and conductive paths of dart leaders, we presented a new method to measure the detailed structure and stepping dynamics of upward channels created by IC initial leaders. The IC initial leaders propagate in an upward but tilted stepped process, with step length and interstep time interval of 295 m and 1.05 ms, respectively. Beyond the basic measurements we report from the combination of initial breakdown pulses and subsequent dart leaders, the stepping structure and dynamics of IC initial upward leaders have two important implications for the leader extension process and leader-associated phenomena.

One is the basic classification of the IBPs into those relating to channel extension and those from nonpropagating branches during the IC initial leaders. The average step time interval measured here is 1.05 ms. This is nearly 2 times longer than the average pulse time interval (0.56 ms) and also much longer than that measured from the CG leader steps [*Qie and Kong*, 2007; *Biagi et al*., 2014; *Stolzenburg et al*., 2014]. Previous observations suggested that pulses during the downward negative leaders of CG flashes were accompanied by luminous branches [*Hill et al.*, 2011; *Lu et al.*, 2012; *Stolzenburg et al.*, 2014], which are associated with leader steps, and even nonpropagating branches. Luminous branches can also be seen from cloud-to-air negative leaders [*Edens et al*., 2014] and bolt-from-the-blue lightning [*Lu and Walden-Newman*, 2009]. Thus, they can be expected for IC initial leaders that are located deep inside the clouds where more complicated ambient electrical fields exist. If each branch was associated with leader pulse, then we would expect a longer channel interstep interval than leader pulse interval, and this is what we measured in this study. We suggest that nearly half of the detectable IBPs do not contribute to the main upward channel extension but may be related to nonpropagating branches. Note that a high-amplitude IBP is more likely to be involved in the main channel extension than a smaller pulse.

In addition, as illustrated in Figures 1 and 2 and Table 1, most of the individual leader steps and the whole initial leader channels are tilted away from vertical from less than ten degrees to a few tens of degrees. This shows the main geometry of the IC initial leader progression and therefore indicates the existence of a significant tilt to the local electric field. We suggest that this has some implications for the observation of leader-associated high-energy radiation phenomena, such as terrestrial gamma ray flashes (TGFs), which are intimately linked to IC initial leaders [e.g., *Lu et al*., 2010; *Marshall et al*., 2013; *Cummer et al*., 2015, and references therein]. Currently, nearly all reported TGFs have been detected by satellite-based high-energy photon detectors, and it has been found that TGF photons can typically be observed when the space-based detector is located above the source within a cone of ~30° to 45° half angle [*Dwyer and Smith*, 2005; *Briggs et al*., 2011; *Gjesteland et al*., 2011]. Since TGFs are generated during the progression of IC initial leaders, the tilted leader stepping and local electric field could result in tilted TGFs, typically by 10–20°, which probably confines the main orientation for the coned beam of gamma ray photons. And thus, in addition to the scatter and attenuation of photons, the geometry of TGF associating IC initial leader or channel could also have an effect on the position-dependent observation of TGFs from space-based detectors.

Acknowledgments
The authors would like to acknowledge support from the National Science Foundation Dynamic and Physical Meteorology program through grant ATM-1047588 and the DARPA Nimbus program through grants HR0011-10-1-0059. We are grateful to Jan Hermans and his wife for providing accommodation for our LF data acquisition equipment. The authors would like to thank all the colleagues who participated in the field experiments. The processing method is fully described in the manuscript, and the LF data for the events are available by request. The authors would like to thank Abram R. Jacobson and another anonymous reviewer for the constructive comments and suggestions to improve the paper.

References

Behnke, S. A., R. J. Thomas, P. R. Krehbiel, and W. Rison (2005), Initial leader velocities during intracloud lightning: Possible evidence for a runaway breakdown effect, *J. Geophys. Res.*, *110*, D10207, doi:10.1029/2004JD005312.

Betz, H. D., K. Schmidt, P. Oettinger, and M. Wirz (2004), Lightning detection with 3-D discrimination of intracloud and cloud-to-ground discharges, *Geophys. Res. Lett.*, *31*, L11108, doi:10.1029/2004GL019821.

Biagi, C. J., M. A. Uman, J. D. Hill, and D. M. Jordan (2014), Negative leader step mechanisms observed in altitude triggered lightning, *J. Geophys. Res. Atmos.*, *119*, 8160–8168, doi:10.1002/2013JD020281.

Bitzer, P. M., H. J. Christian, M. Stewart, J. Burchfield, S. Podgorny, D. Corredor, J. Hall, E. Kuznetsov, and V. Franklin (2013), Characterization and applications of VLF/LF source locations from lightning using the Huntsville Alabama Marx Meter Array, *J. Geophys. Res. Atmos.*, *118*, 3120–3138, doi:10.1002/jgrd.50271.

Briggs, M. S., et al. (2011), Electron-positron beams from terrestrial lightning observed with Fermi GBM, *Geophys. Res. Lett.*, *38*, L02808, doi:10.1029/2010GL046259.

Cummer, S. A., F. Lyu, M. S. Briggs, G. Fitzpatrick, O. J. Roberts, and J. R. Dwyer (2015), Lightning leader altitude progression in terrestrial gamma ray flashes, *Geophys. Res. Lett.*, *42*, doi:10.1002/2015GL065228.

Dong, W., X. Liu, Y. Zhang, and G. Zhang (2002), Observation on the leader-return stroke of cloud-to-ground lightning with the broadband interferometer, *Sci. China Earth Sci.*, *45*(3), 259–269.

Dwyer, J. R., and D. M. Smith (2005), A comparison between Monte Carlo simulations of runaway breakdown and terrestrial gamma ray flash observations, *Geophys. Res. Lett.*, *32*, L22804, doi:10.1029/2005GL023848.

Edens, H. E., K. B. Eack, W. Rison, and S. J. Hunyady (2014), Photographic observations of streamers and steps in a cloud-to-air negative leader, *Geophys. Res. Lett.*, *41*, 1336–1342, doi:10.1002/2013GL059180.

Gjesteland, T., N. Østgaard, A. B. Collier, B. E. Carlson, M. B. Cohen, and N. G. Lehtinen (2011), Confining the angular distribution of terrestrial gamma ray flash emission, *J. Geophys. Res.*, *116*, A11313, doi:10.1029/2011JA016716.

Hill, J. D., M. A. Uman, and D. M. Jordan (2011), High-speed video observations of a lightning stepped leader, *J. Geophys. Res.*, *116*, D16117, doi:10.1029/2011JD015818.

Karunarathne, S., T. C. Marshall, M. Stolzenburg, N. Karunarathna, L. E. Vickers, T. A. Warner, and R. E. Orville (2013), Locating initial breakdown pulses using electric field change network, *J. Geophys. Res. Atmos.*, *118*, 7129–7141, doi:10.1002/jgrd.50441.

Kawasaki, Z., R. Mardiana, and T. Ushio (2000), Broadband and narrowband RF interferometers for lightning observations, *Geophys. Res. Lett.*, *27*, 3189–3192, doi:10.1029/1999GL011058.

Krehbiel, P. R., J. A. Riousset, V. P. Pasko, R. J. Thomas, W. Rison, M. A. Stanley, and H. E. Edens (2008), Upward electrical discharges from thunderstorms, *Nat. Geosci.*, *1*, 233–237, doi:10.1038/ngeo162.

Liu, H., W. Dong, T. Wu, D. Zheng, and Y. Zhang (2012), Observation of compact intracloud discharges using VHF broadband interferometers, *J. Geophys. Res.*, *117*, D01203, doi:10.1029/2011JD016185.

Lu, G., and W. Walden-Newman (2009), Analysis of the video recordings of an aborted upward leader at daytime from a "Bolt-from-the-Blue" discharge, *J. Lightning Res.*, *1*, 22–27, doi:10.2174/1652803400901010022.
Lu, G., R. J. Blakeslee, J. Li, D. M. Smith, X.-. M. Shao, E. W. McCaul, D. E. Buechler, H. J. Christian, J. M. Hall, and S. A. Cummer (2010), Lightning mapping observation of a terrestrial gamma ray flash, *Geophys. Res. Lett.*, *37*, L11806, doi:10.1029/2010GL043494.
Lu, G., R. Jiang, X. Qie, H. Zhang, Z. Sun, M. Liu, Z. Wang, and K. Liu (2014), Burst of intracloud current pulses during the initial continuous current in a rocket-triggered lightning flash, *Geophys. Res. Lett.*, *41*, 9174–9181, doi:10.1002/2014GL062127.
Lu, W., L. Chen, Y. Zhang, Y. Ma, Y. Gao, Q. Yin, S. Chen, Z. Huang, and Y. Zhang (2012), Characteristics of unconnected upward leaders initiated from tall structures observed in Guangzhou, *J. Geophys. Res.*, *117*, D19211, doi:10.1029/2012JD018035.
Lyu, F., S. A. Cummer, R. Solanki, J. Weinert, L. McTague, A. Katko, J. Barrett, L. Zigoneanu, Y. Xie, and W. Wang (2014), A low-frequency near-field interferometric-TOA 3-D Lightning Mapping Array, *Geophys. Res. Lett.*, *41*, 7777–7784, doi:10.1002/2014GL061963.
Marshall, T., M. Stolzenburg, S. Karunarathne, S. Cummer, G. Lu, H. D. Betz, M. Briggs, V. Connaughton, and S. Xiong (2013), Initial breakdown pulses in intracloud lightning flashes and their relation to terrestrial gamma ray flashes, *J. Geophys. Res. Atmos.*, *118*, 10,907–10,925, doi:10.1002/jgrd.50866.
Mazur, V. (1989), Triggered lightning strikes to aircraft and natural intracloud discharges, *J. Geophys. Res.*, *94*(D3), 3311–3325, doi:10.1029/JD094iD03p03311.
Montanyà, J., O. van der Velde, and E. R. Williams (2015), The start of lightning: Evidence of bidirectional lightning initiation, *Sci. Rep.*, *5*, 15,180, doi:10.1038/srep15180.
Proctor, D. E. (1981), VHF radio pictures of cloud flashes, *J. Geophys. Res.*, *86*, 4041–4071, doi:10.1029/JC086iC05p04041.
Proctor, D. E., R. Uytenbogaardt, and B. M. Meredith (1988), VHF radio pictures of lightning flashes to ground, *J. Geophys. Res.*, *93*, 12,683–12,727, doi:10.1029/JD093iD10p12683.
Qie, X., and X. Kong (2007), Progression features of a stepped leader process with four grounded leader branches, *Geophys. Res. Lett.*, *34*, L06809, doi:10.1029/2006GL028771.
Qiu, S., B. Zhou, L. Shi, W. Dong, Y. Zhang, and T. Gao (2009), An improved method for broadband interferometric lightning location using wavelet transforms, *J. Geophys. Res.*, *114*, D18211, doi:10.1029/2008JD011655.
Rhodes, C. T., X. M. Shao, P. R. Krehbiel, R. J. Thomas, and C. O. Hayenga (1994), Observations of lightning phenomena using radio interferometry, *J. Geophys. Res.*, *99*, 13,059–13,082, doi:10.1029/94JD00318.
Rison, W., R. J. Thomas, P. R. Krehbiel, T. Hamlin, and J. Harlin (1999), A GPS-based three-dimensional lightning mapping system: Initial observations in central New Mexico, *Geophys. Res. Lett.*, *26*, 3573–3576.
Shao, X. M., and P. R. Krehbiel (1996), The spatial and temporal development of intracloud lightning, *J. Geophys. Res.*, *101*, 26,641–26,668.
Stock, M. G., M. Akita, P. R. Krehbiel, W. Rison, H. E. Edens, Z. Kawasaki, and M. A. Stanley (2014), Continuous broadband digital interferometry of lightning using a generalized cross-correlation algorithm, *J. Geophys. Res. Atmos.*, *119*, 3134–3165, doi:10.1002/2013JD020217.
Stolzenburg, M., T. C. Marshall, S. Karunarathne, N. Karunarathna, and R. E. Orville (2014), Leader observations during the initial breakdown stage of a lightning flash, *J. Geophys. Res. Atmos.*, *119*, 12,198–12,221, doi:10.1002/2014JD021994.
Sun, Z., X. Qie, R. Jiang, M. Liu, X. Wu, Z. Wang, G. Lu, and H. Zhang (2014), Characteristics of a rocket-triggered lightning flash with large stroke number and the associated leader propagation, *J. Geophys. Res. Atmos.*, *119*, 13,388–13,399, doi:10.1002/2014JD022100.
Wang, Y., X. Qie, D. Wang, M. Liu, D. Su, Z. Wang, D. Liu, Z. Wu, Z. Sun, and Y. Tian (2016), Beijing Lightning Network (BLNET) and the observation on preliminary breakdown processes, *Atmospheric Research*, *171*, 121–132, doi:10.1016/j.atmosres.2015.12.012.
Winn, W. P., G. D. Aulich, S. J. Hunyady, K. B. Eack, H. E. Edens, P. R. Krehbiel, W. Rison, and R. G. Sonnenfeld (2011), Lightning leader stepping, K changes, and other observations near an intracloud flash, *J. Geophys. Res.*, *116*, D23115, doi:10.1029/2011JD015998.
Wu, T., S. Yoshida, Y. Akiyama, M. Stock, T. Ushio, and Z. Kawasaki (2015), Preliminary breakdown of intracloud lightning: Initiation altitude, propagation speed, pulse train characteristics and step length estimation, *J. Geophys. Res. Atmos.*, *120*, doi:10.1002/2015JD023546.
Yoshida, S., T. Wu, T. Ushio, K. Kusunoki, and Y. Nakamura (2014), Initial results of LF sensor network for lightning observation and characteristics of lightning emission in LF band, *J. Geophys. Res. Atmos.*, *119*, 12,034–12,051, doi:10.1002/2014JD022065.
Zhang, G., Y. Wang, X. Qie, T. Zhang, Y. Zhao, Y. Li, and D. Cao (2010), Using lightning locating system based on time-of-arrival technique to study three-dimensional lightning discharge processes, *Sci. China Earth Sci.*, *53*, 591–602, doi:10.1007/s11430-009-0116-x.